

# Entropic exponents of grafted lattices stars

EJ Janse van Rensburg<sup>1</sup>

<sup>1</sup>*Department of Mathematics and Statistics, York University,  
Toronto, Ontario M3J 1P3, Canada (Email: rensburg@yorku.ca)*

(Dated: July 19, 2022)

The surface entropic exponents of half-space lattice stars grafted at their central nodes in a hard wall are estimated numerically using the PERM algorithm. In the square half-lattice the exact values of the exponents are verified, including Barber's scaling relation and a generalisation for 2-stars with one and two surface loops respectively. This is the relation

$$\gamma_{211} = 2\gamma_{21} - \gamma_{20},$$

where  $\gamma_{21}$  and  $\gamma_{211}$  are the surface entropic exponents of a grafted 2-star with one and two surface loops respectively, and  $\gamma_{20}$  is the surface entropic exponent with no surface loops. This relation is also tested in the cubic half-lattice where surface entropic exponents are estimated up to 5-stars, including many with one or more surface loops. Barber's scaling relation and the relation

$$\gamma_{3111} = \gamma_{30} - 3\gamma_{31} + 3\gamma_{311}$$

are also tested, where the exponents  $\{\gamma_{31}, \gamma_{311}, \gamma_{3111}\}$  are of grafted 3-stars with one, two or three surface loops respectively, and  $\gamma_{30}$  is the surface exponent of grafted 3-stars.

PACS numbers: 82.35.Lr, 82.35.Gh, 61.25.Hq

## INTRODUCTION

The *connectivity* of a polymer network can be represented as an abstract graph  $\mathcal{G}$  of nodes and bonds, where the nodes are branching points in the network, and the bonds represent linear polymers joining the nodes into the network. If the network is embedded in a lattice, then it is a model of the connectivity and the topology of a polymer network in the plane or in a thin layer (if the lattice is two dimensional), or in a good solvent (if the lattice is three dimensional).

If a network with connectivity  $\mathcal{G}$  is embedded in the (hyper)-cubic lattice  $\mathbb{Z}^d$ , then the nodes are located on vertices in the lattice, and the bonds are mutual- and self-avoiding walks joining the nodes. These self-avoiding walks are the *branches* of the network. If  $\mathcal{G}$  is a star graph, then the branches are called *arms*. The embedding is *uniform* or *monodispersed* if all the branches are walks of the same length.

The lattice embedding is a model that quantifies the entropy of the corresponding polymer network. If  $c_n(\mathcal{G})$  is the number of distinct embeddings of the network, counted up to translation (or by fixing a node at the origin), then the usual scaling assumption is

$$c_n(\mathcal{G}) \sim n^{\gamma(\mathcal{G})-1} \mu_d^n \quad (1)$$

where  $\gamma(\mathcal{G})$  is the *entropic exponent* of the network and  $\mu_d$  is the self-avoiding walk growth constant [1, 2] (see references [3, 4], and for lattice stars reference [5]). The best estimates of the growth constants in the square and

cubic lattices are obtained from simulations of the self-avoiding walk, and are

$$\mu_2 = 2.63815853035(2), \quad [6] \quad (2)$$

$$\mu_3 = 4.684039931(27). \quad [7] \quad (3)$$

Uniform lattice star polymers form a particular class of lattice networks that have received significant attention in the literature at least since the 1980s [3–5, 8–11]. If  $s_n^{(f)}$  is the number of uniform lattice stars in  $\mathbb{Z}^d$  with  $f$  arms (these are *f-stars*) with central node at the origin, then by equation (1),

$$s_n^{(f)} \sim n^{\gamma_f-1} \mu_d^n, \quad (4)$$

where  $\gamma_f$  is the *f-star entropic exponent*. High quality numerical results and estimates of the entropic exponents of star polymers were made in references [12–17].

Lattice networks of connectivity  $\mathcal{G}$  grafted to a wall have scaling similar to equation (1). In the hypercubic half-lattice  $\mathbb{Z}_+^d = \{(x_1, x_2, \dots, x_d) \in \mathbb{Z}^d \mid \text{such that } x_d \geq 0\}$  a chosen node of a network is grafted at the origin. Nodes of the network located in the boundary (or hard wall)  $\partial\mathbb{Z}_+^d$  of the half-lattice are *surface nodes*. Depending on the connectivity  $\mathcal{G}$  such networks may have *loops* (circuits which are lattice polygons) as well as *surface loops* (self-avoiding walks with both endpoints in hard wall  $\partial\mathbb{Z}_+^d$  of the half-lattice). For example, in figure 1 we show a schematic of a lattice network in  $\mathbb{Z}_+^2$  with connectivity a lattice 3-star without (left) and with (right) a surface loop.

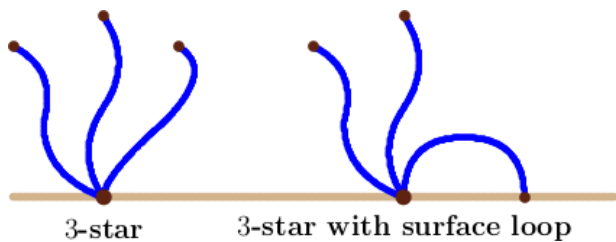


FIG. 1: Schematic of 3-stars in a half-lattice. The central node of the star is attached at the origin in the hard wall (the boundary of the half-lattice). On the right the star has one arm forming a surface loop. The star on the left has no loops or surface loops.

### Vertex exponents, and entropic exponents

The entropic exponents of networks of connectivity  $\mathcal{G}$ , in the full lattice, or in the half-lattice, can be expressed in term of *vertex exponents*  $\sigma_f$  and *surface vertex exponents*  $\sigma'_g$  by

$$\gamma_{\mathcal{G}} = 1 + \sum_f m_f \sigma_f + \sum_g m_g \sigma'_g - c(\mathcal{G}) \nu - \ell(\mathcal{G}) \nu \quad (5)$$

where  $\nu$  is the metric exponent of the self-avoiding walk ( $\nu = 3/4$  in two dimensions [18, 19], and  $\nu = 0.58759700(40)$  in three dimensions [20]). The coefficient  $m_g$  is the number of surface-nodes of degree  $g$  in  $\partial\mathbb{Z}_+^d$ ,  $m_f$  is the number of nodes of degree  $f$  in the bulk lattice,  $c(\mathcal{G})$  is the number of independent circuits in the network, and  $\ell(\mathcal{G})$  is the number of independent surface loops [21, 22]. Testing of equation (5) are limited to self-avoiding walks in a half-lattice [23], and for branched networks, to star polymers in bulk [15–17] and a few cases of branched acyclic networks in bulk [16, 17].

Exact values of the vertex exponents in two dimensions were calculated using conformal invariance techniques [18, 19]. These are

$$\sigma_f = \frac{1}{64} (2-f)(9f+2), \quad \text{and} \quad \sigma'_f = \frac{1}{32} f(2-9f). \quad (6)$$

Using these expressions, the exact values of  $\gamma_{\mathcal{G}}$  are known in the square lattice. For example, putting  $f = 0$  and using equation (5) gives the exact value of the entropic exponent of the self-avoiding walk  $\gamma = 1 + 2\sigma_1 = 43/32$ .

In three dimensions there are  $\epsilon$ -expansion estimates [24] for the vertex exponents. To first order in  $\epsilon$  [21],

$$\sigma_f = \frac{\epsilon}{16} f(2-f) + O(\epsilon^2); \quad (7)$$

$$\sigma'_f = -\frac{1}{2} f + \frac{\epsilon}{16} f(2-f) + O(\epsilon^2). \quad (8)$$

These approximations deteriorate quickly with increasing degrees of the nodes (see for example [17]), but can be used with equation (5) to approximate the entropic exponents  $\gamma_{\mathcal{G}}$  in three dimensions. In the case of the self-avoiding walk, the  $\epsilon$ -expansion estimate  $\gamma = 1 + 2\sigma_1 \approx$

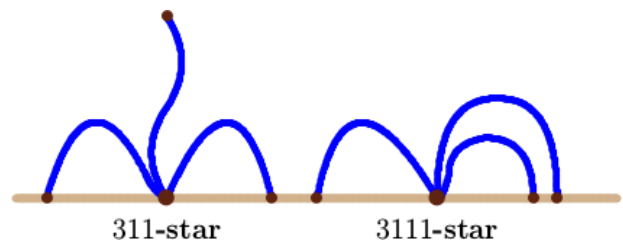


FIG. 2: Schematic illustrations of 311-stars (left) and 3111-stars (right) in a half-lattice. In the half-square lattice the one arm of the 311-star is “screened” from the hard wall by the other two arms with endpoints in the hard wall. In the case of 3111-stars all three arms have endpoints in the hard wall, and the only way to accommodate this is by having one arms located inside the surface loop created by the hard wall and an arm. This makes simulations of 3111-stars in the square half-lattice very challenging. In our PERM simulations we rarely observed these states in the  $10^9$  iterations done.

1.125 compares relatively well with the best numerical estimates  $\gamma = 1.15698(34)$  [25] and  $\gamma = 1.15695300(95)$  [26].

In this paper the focus is on a lattice star in the half-lattice with its central node at the origin, such as schematically illustrated in figure 1. We first introduce notation to distinguish the connectivities of  $f$ -stars in the half-lattice  $\mathbb{Z}_+^d$  efficiently.

Let  $f1^g \equiv f \overbrace{11\dots 1}^g$  denote lattice stars in the half-lattice  $\mathbb{Z}_+^d$  with central node of degree  $f$  located at the origin in the boundary  $\partial\mathbb{Z}_+^d$  (the hard wall), and with  $g \leq f$  arms having their endpoints in the hard wall (and so forming  $g$  surface loops). For example, in figure 1 the cases  $31^0 \equiv 30$  (left) and  $31^1 \equiv 31$  (right) are shown. Similarly,  $31^2 \equiv 311$  denotes 3-stars with central node at the origin and with 2 arms having their end-points in the hard wall (and so forming two surface loops), and  $31^3 \equiv 3111$  denotes 3-stars with three surface loops (see figure 2).

The entropic exponents of half-lattice stars with connectivity  $f1^g$  is denoted by  $\gamma_{f1^g}$ . For example,  $\gamma_{311}$  is the entropic exponent of 3-stars with two arms forming surface loops, and for the cases in figure 1, we have  $\gamma_{30}$  (left) and  $\gamma_{31}$  (right). In terms of equation (5) the entropic exponent of  $f$ -stars with  $g$  surface loops in the half-lattice is given by

$$\gamma_{f1^g} = \gamma_f \underbrace{11\dots 1}_g = 1 + \sigma'_f + (f-g)\sigma_1 + g\sigma'_1 - g\nu. \quad (9)$$

The vertex exponents are given in equation (6) in two dimensions, and are approximated in the  $\epsilon$ -expansion in equations (7) and (8) in three dimensions.

In the case of a self-avoiding walk  $\gamma = 1 + 2\sigma_1$ , and for a walk from the origin in  $\mathbb{Z}_+^d$ ,  $\gamma_1 = 1 + \sigma'_1 + \sigma_1$  (since  $f = 1$  and  $g = 0$ ). If both endpoints are in  $\partial\mathbb{Z}_+^d$ , then  $f = g = 1$

and thus  $\gamma_{11} = 1 + 2\sigma'_1 - \nu$ . Eliminating  $\sigma_1$  and  $\sigma'_1$  gives Barber's scaling relation [27, 28]

$$2\gamma_1 - \gamma_{11} = \gamma + \nu. \quad (10)$$

In  $d = 2$  the sum of the exact values  $\gamma = 43/32$ ,  $\nu = 3/4$  on the right hand side equals the sum of the exact values  $\gamma_1 = 61/64$  [18] and  $\gamma_{11} = -3/16$  [29] on the left hand side. Numerical results are in agreement with these results, namely  $\gamma_1 = 0.945(5)$  and  $\gamma_{11} = -0.19(3)$  [28], and  $\gamma_1 = 0.9551(3)$  [30]. This shows that  $2\gamma_1 - \gamma_{11} = 2.08(4)$  while the exact value is  $\gamma + \nu = 67/32 = 2.09375\dots$

In three dimensions early estimates  $\gamma_1 = 0.687(5)$  and  $\gamma_{11} = -0.38(2)$  [31, 32], and  $\gamma_1 = 0.697(2)$  and  $\gamma_{11} = -0.383(5)$  [33], gave way to the more accurate results  $\gamma_1 = 0.6786(12)$  and  $\gamma_{11} = -0.390(2)$  in reference [23]. The best available estimates can be found in reference [34] where  $\gamma_1$  is estimated, and  $\gamma_{11}$  is estimated from the bridge entropic exponent  $\gamma_b$  using the relation  $\gamma_b = \gamma_{11} + \nu$  [11]. These are  $\gamma_1 = 0.677667(17)$  and  $\gamma_{11} = -0.389245(28)$ . These values give  $2\gamma_1 - \gamma_{11} = 1.744579(62)$  and using the best estimates  $\gamma = 1.15695300(95)$  [26] and  $\nu = 0.58759700(40)$  [20, 35],  $\gamma + \nu = 1.7445500(14)$ . This confirms the Barber scaling relation to very high accuracy. The mean field values of these exponents are  $\gamma = 1$ ,  $\nu = 1/2$ ,  $\gamma_1 = 1/2$  and  $\gamma_{11} = -1/2$  [36, 37].

More generally, one may notice that when  $f \geq 2$ , then the vertex exponents in equation (9) can be eliminated by using an alternating sum and binomial coefficients, so that

$$\sum_{g=0}^f (-1)^g \binom{f}{g} \gamma_{f1^g} = 0. \quad (11)$$

This shows, for example, that  $\gamma_{20} - 2\gamma_{21} + \gamma_{211} = 0$  and  $\gamma_{30} - 3\gamma_{31} + 3\gamma_{311} - \gamma_{3111} = 0$  and so on. The identity

$$\gamma_{20} = \gamma - 1 \quad (12)$$

was noted in reference [21]) and from it and equation (11) with  $f = 2$  it follows that

$$2\gamma_{21} - \gamma_{211} = \gamma - 1. \quad (13)$$

This is a generalisation of Barber's scaling relation (equation (10)).

## NUMERICAL RESULTS

The numerical approaches developed in reference [23] based on the PERM algorithm [15–17, 38, 39], and in particular the flat histogram [40] and the parallel implementations [41] of PERM, can be used to estimate lattice star entropic exponents in  $\mathbb{Z}^d$  (and in  $\mathbb{Z}_+^d$ ) efficiently (see

reference [23] for half-space self-avoiding walk sampling using PERM). In this paper similar approaches are used, except that, in addition to self-avoiding walks grafted at one endpoint in  $\partial\mathbb{Z}_+^d$ ,  $f$ -stars are sampled with their central nodes at the origin in  $\mathbb{Z}_+^d$ . The details of our simulations are shown in table I. An iteration is a started PERM sequence (which may be pruned and enriched by the algorithm). In these simulations the mersenne twister random number generator [42] was used, except in one case as noted in table I, where the Panneton generator in reference [43] was used instead.

TABLE I: PERM simulations

Dimension	Star	Length	Threads	Iter/Thread	Iterations
$d = 2$	1	10000	4	$2.5 \times 10^8$	$10^9$
	2	16000	4	$2.5 \times 10^8$	$10^9$
	3	15900	4	$2.5 \times 10^8$	$10^9$
$d = 3$	1	10000	4	$2.5 \times 10^8$	$10^9$
	1*	10000	8	$1.25 \times 10^8$	$4.04 \times 10^8$
	2	10000	4	$2.5 \times 10^8$	$10^9$
	3	9900	6	$1.666 \times 10^8$	$10^9$
	4	10000	4	$2.5 \times 10^8$	$10^9$
	5	12500	4	$2.5 \times 10^8$	$10^9$

\* – Panneton generator [43]

In each simulation the data were sieved by collecting data on stars separately by number surface loops. Thus, the algorithm produced data on  $s_n^{(f)}(g)$ , the number of stars with central node of degree  $f$  at the origin in the half-lattice  $\mathbb{Z}_+^d$ , and with  $g$  arms forming surface loops. The scaling of  $s_n^{(f)}(g)$  is

$$s_n^{(f)}(g) \sim n^{\gamma_{f1^g}-1} \mu_d^n (1 + B/n + C/n^\Delta + \dots), \quad (14)$$

where  $\Delta$  is the (first) self-avoiding walk confluent correction exponent which has value  $\Delta = 3/2$  if  $d = 2$  [19, 44, 45] and  $\Delta = 0.528(8)$  if  $d = 3$  [20]. Dividing by  $\mu_d^n n^{\gamma_{f1^g}-1}$  and taking logarithms give

$$\log \left( \frac{s_n^{(f)}(g)}{\mu_d^n n^{\gamma_{f1^g}-1}} \right) = \begin{cases} A + B/n + \dots, & \text{if } d = 2; \\ A + B/n^\Delta + \dots, & \text{if } d = 3, \end{cases} \quad (15)$$

where the logarithms on the right hand side were expanded assuming  $n$  is large. The best value of  $\gamma_{f1^g}$  and a confidence interval on it can be determined by plotting the left hand side against  $1/n$  if  $d = 2$ , and against  $1/n^\Delta$  if  $d = 3$ . This approach was developed in reference [23] where it was used effectively for estimating  $\gamma_1$  and  $\gamma_{11}$  using PERM simulations in the cubic half-lattice. See also references [15–17].

**Two dimensions:** In the square half-lattice the best estimate of  $\mu_2$  (see equation (2)) was used in equation (15). The top panel of figure 1 shows the data for self-avoiding walks grafted to the hard wall (these are 10-stars in our notation) with entropic exponent  $\gamma_1 \equiv \gamma_{10}$ . The

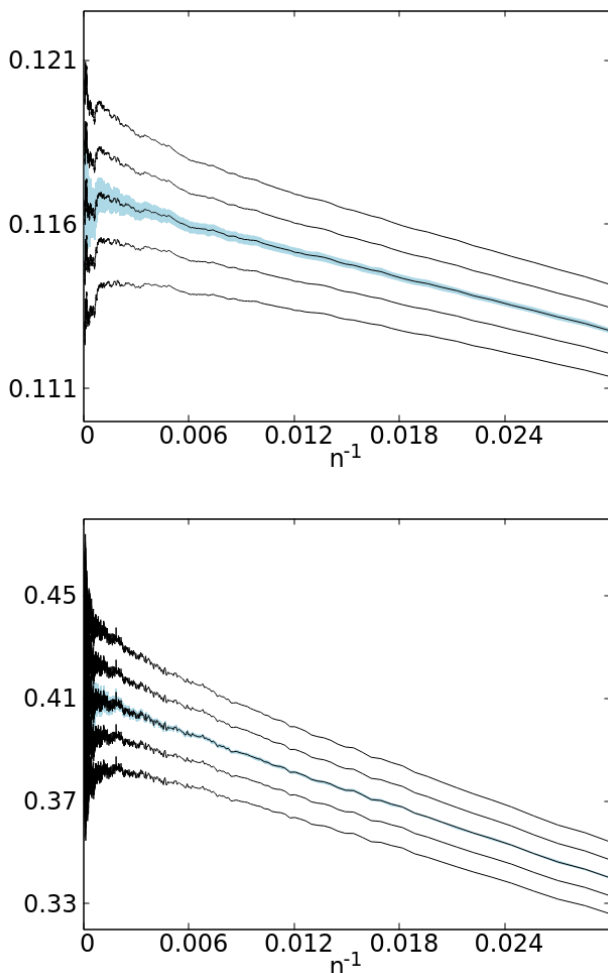


FIG. 3: Determining  $\gamma_1$  and  $\gamma_{11}$  in the square lattice by plotting the left-hand side of equation (15) as a function of  $1/n$ . The middle curve is obtained by selecting that value of the exponent giving a straight line. In each panel a shaded envelope (more visible in the top panel) on the middle curve gives the confidence interval on the raw data. (Top panel) The middle curve is plotted with  $\gamma_1 = 0.95325$  against  $1/n$ . A confidence interval  $\sigma = 0.00020$  is obtained by adding and subtracting  $\sigma$  from  $\gamma_1$ . The top two curves have an increasing upwards tendency as the  $y$ -axis is approached, and the bottom two curves similarly have a downwards tendency. This gives the best (rounded) estimate  $\gamma_1 = 0.9533 \pm 0.0002$ . (Bottom panel) A similar analysis to determine  $\gamma_{11}$ . This gives  $\gamma_{11} = -0.188 \pm 0.002$ .

middle curve shows the confidence interval on the data as a shaded envelope. There are odd-even parity effects in these plots, but they were dealt with by only plotting data for even values of  $n$ .

The best estimate of  $\gamma_1$  was obtained fixing its value to straighten the graph in figure 3. An error bar on the best estimate was determined by varying the value of  $\gamma_1$  to produce the other curves in the figure. These curves are either convex or concave as the  $y$ -axis is approached, and this curving becomes apparent when  $\gamma_1$  is changed

by  $\epsilon = 0.00020$  in either direction. Thus, we select as our error bar on  $\gamma_1$  this value of  $\epsilon$ , giving our best estimate

$$\gamma_1 = 0.95325 \pm 0.00020. \quad (16)$$

The estimate for  $\gamma_{11}$  was similarly obtained using the data of grafted self-avoiding walks with their endpoints in the hard wall forming a surface loop (these are 11-stars in our notation). The results of the analysis are shown in the bottom panel of figure 3. Our best estimate is

$$\gamma_{11} = -0.1875 \pm 0.0020. \quad (17)$$

With these results one may test Barber's scaling relation. Note that

$$2\gamma_1 - \gamma_{11} = 2.094 \pm 0.003. \quad (18)$$

The exact value is  $\gamma + \nu = 43/32 + 3/4 = 67/32 = 2.09375$ . The absolute difference from the estimate above is 0.00025, a factor of 10 smaller than the stated error bar of 0.003. This result is a strong numerical verification of Barber's scaling relation in two dimensions.

TABLE II: Half square lattice entropic exponents

$\gamma_g$	Exact	Literature	This work
$\gamma_1$	0.953125	0.945(5) [28] 0.9551(3) [30]	0.9533(2)
$\gamma_{11}$	-0.1875	-0.19(3) [28]	-0.188(2)
$\gamma_{20}$	0.34375		0.344(1)
$\gamma_{21}$	-0.796875		-0.796(2)
$\gamma_{211}$	-1.9375		-1.94(3)
$\gamma_{211}$	-1.9375		-1.94(5)*
$\gamma_{211}$	-1.9375		-1.93(4)†
$\gamma_{30}$	-0.828125		-0.827(2)
$\gamma_{31}$	-1.96875		-1.969(4)
$\gamma_{311}$	-3.109375		-3.11(1)
$\gamma_{3111}$	-4.25		-4.25(5)*

\* - Calculated by equation (11)

† - Calculated by equation (13)

The remaining data for 2-stars and 3-stars were similarly analysed to obtain estimates of the exponents  $\gamma_{21g}$  and  $\gamma_{31g}$ . The results are shown in table II. Observe that there are no numerical estimates in the literature for these exponents. These estimates are consistent, within error bars, with the (known) exact values in two dimensions. This both confirms, on the one hand, that the exact results are correct, and on the other hand, that the numerical methods in this paper produce high quality estimates of the entropic exponents. Testing equation (13) using our numerical values give

$$2\gamma_{21} - \gamma_{211} = 0.348 \pm 0.034 \quad (19)$$

and the exact value of  $\gamma_{-1} = 11/32 = 0.34375$  is well inside the stated error bar. The estimate for  $\gamma_{20}$  also verifies the identity in equation (12).

The exceptional case is for 3111-stars, namely 3-stars with their central node at the origin in the half square lattice and with each arm from the central node having its endpoint in the hard wall (see figure 2). In this case the data were too sparse to analyse. In general very few 3111-star conformations were encountered in our simulation because one arm will have to be accommodated inside a surface loop formed by another and the hard wall (as illustrated schematically in figure 2). What data obtained were not inconsistent with the exact value  $\gamma_{3111} = -4.25$ .

A numerical estimate of  $\gamma_{3111}$  can be obtained from the other three 3-star exponents using equation (11), namely

$$\gamma_{3111} = \gamma_{30} - 3\gamma_{31} + 3\gamma_{311} = -4.25 \pm 0.05, \quad (20)$$

where we used the results in table II, and added the error bars to find a confidence interval.

Overall, one can conclude that equation (9), and the exact values of the entropic exponents in two dimensions, are supported by our numerical results.

TABLE III: Half cubic lattice entropic exponents

$\gamma_{\mathcal{G}}$	$\epsilon^1$ -approx	Literature	This work
$\gamma_1$	0.625	0.679(2) [33]	0.6785(8)
		0.687(5) [31, 32]	
		0.6786(12) [23]	0.6776(10) <sup>‡</sup>
		0.677667(17) [34]	
$\gamma_{11}$	-0.463	-0.383(5) [33]	-0.389(3)
		-0.38(2) [31, 32]	
		-0.390(2) [23]	-0.394(5) <sup>‡</sup>
		-0.389245(28) [34]	
$\gamma_{20}$	0.125	0.15698(34) [21, 25]	0.154(3)
$\gamma_{21}$	-0.963		-0.918(8)
$\gamma_{211}$	-2.050		-2.02(8)
$\gamma_{211}$	-2.050		-1.99(2) <sup>*</sup>
$\gamma_{211}$	-2.050		-1.99(2) <sup>†</sup>
$\gamma_{30}$	-0.500		-0.521(2)
$\gamma_{31}$	-1.588		-1.59(2)
$\gamma_{311}$	-2.675		-2.68(7)
$\gamma_{3111}$	-3.763		-3.9(6)
$\gamma_{3111}$	-3.763		-3.8(2) <sup>*</sup>
$\gamma_{40}$	-1.250		-1.325(4)
$\gamma_{41}$	-2.338		-2.406(8)
$\gamma_{411}$	-3.425		-3.48(4)
$\gamma_{4111}$	-4.513		-4.6(2)
$\gamma_{41111}$	-5.600		-5.8(1.1) <sup>*</sup>
$\gamma_{50}$	-2.125		-2.243(4)
$\gamma_{51}$	-3.213		-3.318(7)
$\gamma_{511}$	-4.300		-4.41(4)
$\gamma_{5111}$	-5.388		-5.5(2)

\* – Calculated by equation (11)

† – Calculated by equation (13)

‡ – Panneton random number generator [43]

**Three dimensions:** In the cubic lattice corrections to scaling are dominated by the confluent correction term which is of the form  $C/n^\Delta$  (see equation (14)). There is

a competing, faster decaying, analytic correction  $B/n$ , or even higher order confluent corrections, which may impact an analysis using equation (15), in particular at small values of  $n$ . Our approach here is based on the methods developed in reference [23], and we will be plotting the left hand of equation (15) against  $n^{-\Delta}$  where  $\Delta$  is fixed at its best estimate  $\Delta = 0.528(8)$  [20]. Unlike in the square lattice, the confluent correction decays slowly, and competing higher order corrections may impact the analysis at small values of  $n$ . Therefore, the aim here is to find a linear plot at large values of  $n$ , discarding data at small  $n$ . In addition, there are, like in the square lattice, odd-even parity effects in the data, and we dealt with these by only plotting data for even values of  $n$ .

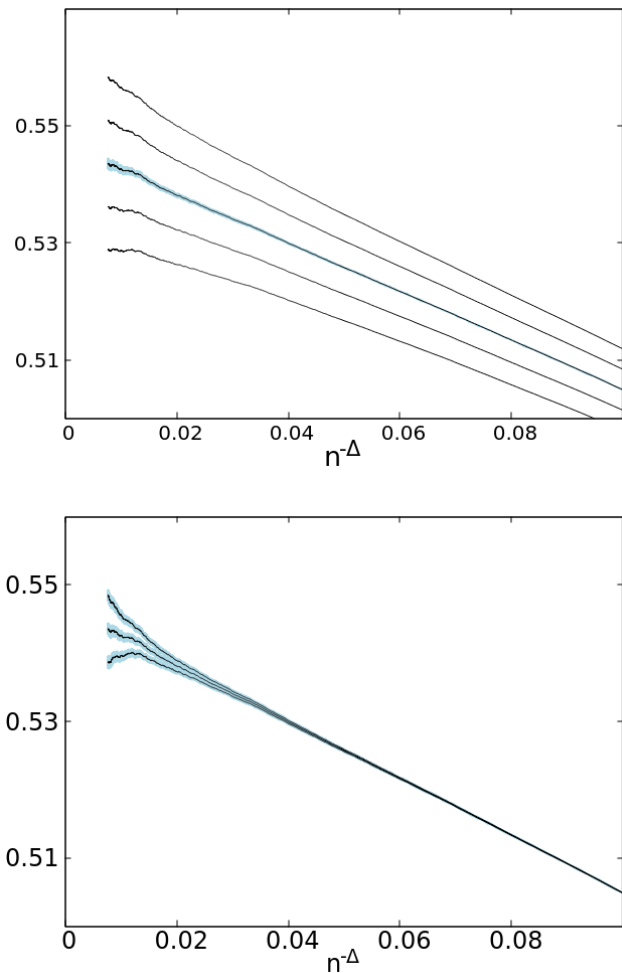


FIG. 4: Determining the best value of  $\gamma_1$ . In the top panel equation (15) was plotted with  $\Delta = 0.528$  and  $\mu_3 = 4.684039931 - \delta$ , where  $\delta = 2.3 \times 10^{-6}$ . The effect of minor changes in the plots due to changes in  $\mu_3$  are shown in the bottom panel. The top curve is for  $\mu_3$  equal to its best value in equation (3), the middle curve for  $\mu_3 - \delta$ , and the bottom curve for  $\mu_3 - 2\delta$ .

Plotting equation (15) to determine  $\gamma_1$  gave graphs which were typically first concave (at small values of  $n$ )

and then turning convex at large values of  $n$ . A linear graph can be obtained by making minor changes in the estimate of  $\mu_3$  and this gives the best estimate

$$\gamma_1 = 0.6745 \pm 0.0008. \quad (21)$$

This estimate was obtained by determining that value of  $\gamma_1$  that straightens the graph when equation (15) was plotted using the data. In this case its final value was insensitive to small changes in the value of  $\mu_3$  from its best estimate in equation (3), and also with small changes in  $\Delta$  within its error bars. However, it was not possible to find a straight graph of the data without changing the value of  $\mu_3$  in minor ways from that in equation (3). Following the approach in reference [23] the effects of these small changes in  $\mu_3$  are shown in the bottom panel of figure 4, where our data are plotted with  $\gamma_1$  fixed at its best value in equation (21), but with the growth constant fixed at  $\mu_3 - k\delta$  where  $k = 0, 1, 2$  and  $\delta = 2.3 \times 10^{-6}$ . If  $k = 0$ , then the curvature is upwards as the  $y$ -axis is approached. The bottom downwards curvative is seen for  $k = 2$ , while the best fit is for  $k = 1$ .

These results do *not* imply that the estimate in equation (3) is suspect, but instead expose limitations in the data in this paper – if the purpose was to estimate  $\mu_3$  from the data obtained here, then one would at best expect to do this to an accuracy of  $O(2.3 \times 10^{-6})$ . In addition, changing  $\mu_3$  from its best value introduces an extra degree of freedom in the analysis, and may give biased estimates of the exponents. In order to avoid this possibility, we fixed the value of  $\mu_3$  at its best known estimate, and then proceeded with curve fitting while discarding data at small values of  $n$ .

The analysis giving the estimate in equation (21) relies almost exclusively on data with  $0.02 \leq n^{-\Delta} \leq 0.10$  (as seen in the bottom panel of figure 4). This corresponds to  $78 \leq n \leq 1650$ , while data with  $n > 1650$  are compensated by the small change in the value of  $\mu_3$ . This, however, cannot be the best way of extracting a good estimate of  $\gamma_1$ , and more care is needed. In particular, one should rely on large values of  $n$  in the analysis, since corrections to scaling are reduced with increasing  $n$ . In addition, changes in the value of  $\mu_3$  introduces an additional degree of freedom in the analysis, and it primarily affects data at large  $n$ . Thus, the analysis was repeated, but without changes in the value of  $\mu_3$ , and discarding data with  $n \leq 766$ . This gives the results in figure 5. The middle curve corresponds to the best estimate of  $\gamma_1$ :

$$\gamma_1 = 0.6785 \pm 0.0008. \quad (22)$$

The two top curves are convex, while the two bottom curves are concave, and give the estimated error bar above. Since this estimate is based on data for larger values of  $n$ , it is taken as the best estimate of this exponent.

We have listed our best estimate for  $\gamma_1 = 0.6785(8)$  in table III, where we also compare it to earlier estimates in

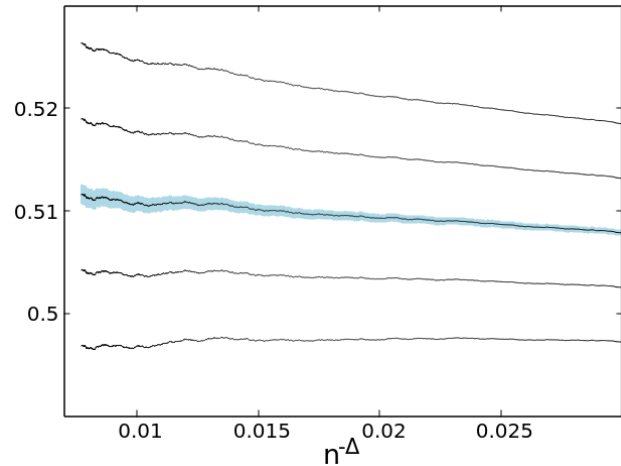


FIG. 5: Determining the best value of  $\gamma_1$ . The middle curve is a plot of equation (15) as a function of  $1/n^\Delta \in [0.007, 0.03]$  with  $\Delta = 0.528$  and  $\mu_3 = 4.684039931$ . This gives the estimate  $\gamma_1 = 0.6785(8)$ . The top two graphs are plotted using  $\gamma_1 + k\epsilon$  with  $k = 1, 2$  where  $\epsilon = 0.0008$ , while the bottom two are plots with  $k = -1, -2$ .

the literature. The best available estimate is in reference [34]. This estimate excludes our best estimate from its (very small) error bar. Conversely, that estimate is well within the error bar in equation (22). Sources of a systematic error in our estimate may be due to the choice of random number generator (in this paper we used the mersenne twister for 64 bit architecture [42]), or due to limitations in carrying significant digits along in the simulation (we used long double (80-bit) precision in the C programming language). We also used gnuplot [46] to analyse the data, and it also has finite precision. We avoided large numbers in our simulation by only storing the ratio  $s_n^{(f)}(g)/\mu_3^n$  in our programs and data files. Repeated division by  $\mu_3$  during the simulation may also introduce rounding errors which accumulate during the simulation.

The value of the surface loop exponent  $\gamma_{11}$  was similarly estimated (figure 6). The best estimate consistent with our data is

$$\gamma_{11} = -0.389 \pm 0.003. \quad (23)$$

Barber's scaling relation can be tested in three dimensions by the results in equations (21) and (23). The best available estimate of the numerical estimate of the metric exponent of self-avoiding walks is  $\nu = 0.58759700(40)$  [20, 35] and of the entropic exponent  $\gamma = 1.15695300(95)$  [26]. Adding these gives  $\gamma + \nu = 1.7445500(14)$ . Our results give

$$2\gamma_1 - \gamma_{11} = 1.746(5). \quad (24)$$

This result includes the sum  $\gamma + \nu$  inside its error bar, and so is consistent with the Barber scaling relation in three dimensions.

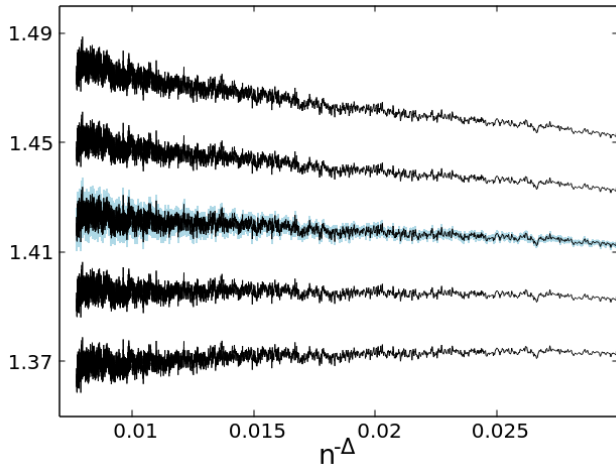


FIG. 6: Determining the best value of  $\gamma_{11}$ . The middle curve is a plot of equation (15) as a function of  $1/n^\Delta$  with  $\Delta = 0.528$  and  $\mu_3 = 4.684039931$ . This gives the estimate  $\gamma_{11} = -0.3893$ . The top two graphs are plotted using  $\gamma_{11} + k\epsilon$  with  $k = 1, 2$  where  $\epsilon = 0.0030$ , while the bottom two are plots with  $k = -1, -2$ .

These results were retested by performing simulations using an alternative random number generator (the Paneton generator [43]). The results are shown in table III where  $\gamma_1 = 0.6776(10)$  and  $\gamma_{11} = -0.394(5)$ . This gives  $2\gamma_1 - \gamma_{11} = 1.749(7)$ , again consistent with the Barber scaling relation and with equation (24).

Plotting our data for grafted  $f$ -stars with  $2 \leq f \leq 5$  produced graphs which do not straighten at the best value of  $\gamma_{f1g}$ . Instead, the locus of the data points were typically concave at small values of  $n$ , even as it straightens as  $n$  increases. This again suggests that higher order corrections to scaling are complicating the analysis. Since the slowest decaying correction is  $C/n^\Delta$ , and it becomes dominant as  $n$  is increased, the exponents were estimated by focussing on the largest values of  $n$  as before. That is, by using equation (15) the exponent is estimated by setting it to straighten the curve at the largest values of  $n$ , even if there is a remaining curvature seen at the smallest values of  $n$ .

In figure 7 the result for  $\gamma_{20}$  is shown. These graphs were obtained by using the best estimate obtained from our data and give

$$\gamma_{20} = 0.154 \pm 0.003. \quad (25)$$

The best estimate of  $\gamma_{20}$  in the literature is obtained by noting from equation (12) that that  $\gamma_{20} = \gamma - 1$  and using the best estimate  $\gamma = 1.15695300(95)$  [26]. This shows that  $\gamma_{20} = 0.15695300(95)$  and this is well within the stated error bar of the estimate in equation (25). Conversely, these results also support the identity in equation (12) in three dimensions.

The analysis for  $\gamma_{21}$  is shown in figure 8. These graphs are for  $573 \leq n \leq 10000$ . Observe that there remains a

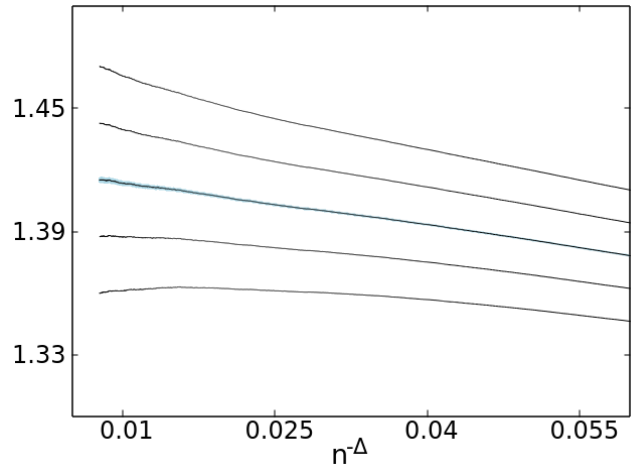


FIG. 7: Estimating  $\gamma_{20}$  by plotting the left hand side of equation (15) as a function of  $n^{-\Delta}$  for  $206 \leq n \leq 10000$ . The middle graph corresponds to the best estimate  $\gamma_{20} = 0.154 \pm 0.003$ , while the top two curves, and the bottom two curves, are used to determine the confidence interval.

minor concavity in the middle curve at the largest values of  $n^{-\Delta}$  but that the curves straighten as  $n^{-\Delta}$  decreases when  $n$  approaches  $n = 10,000$ . The top two curves are convex, and the bottom two curves are concave. This gives the best value of  $\gamma_{21}$ :

$$\gamma_{21} = -0.918 \pm 0.008. \quad (26)$$

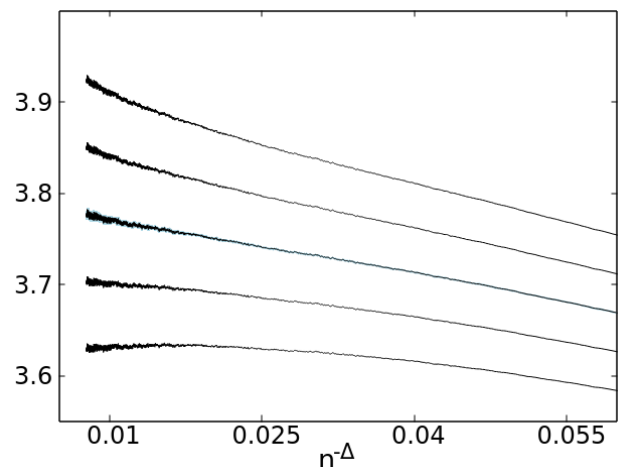


FIG. 8: Plotting equation (15) against  $n^{-\Delta}$  for  $573 \leq n \leq 10000$  to determine  $\gamma_{21}$ .

The estimates of  $\gamma_{20}$  and  $\gamma_{21}$  in equations (24) and (26) can be used to predict  $\gamma_{211}$  using equation (11). This gives

$$\gamma_{211} = 2\gamma_{21} - \gamma_{20} = -1.99 \pm 0.02. \quad (27)$$

Determining  $g_{211}$  directly from the data is complicated by poor sampling at large  $n$ . Examination of the data shows

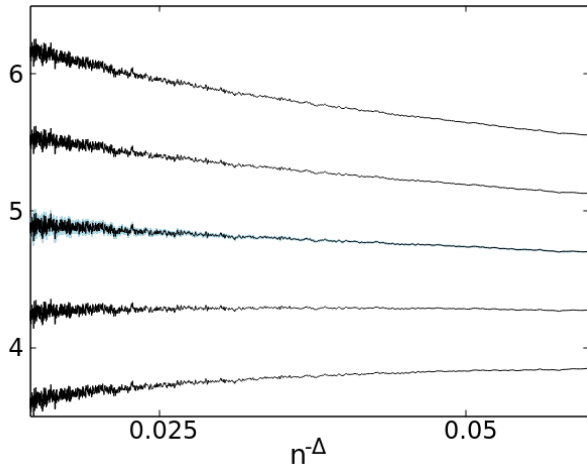


FIG. 9: Plotting equation (15) against  $n^{-\Delta}$  for  $37 \leq n \leq 2946$  to determine  $\gamma_{211}$ .

reasonable sampling for  $n \leq 2500$ , and poor sampling for  $n \geq 3000$ . Plotting equation (15) for  $37 \leq n \leq 2846$  gives figure 9 which unambiguously gives the estimate

$$\gamma_{211} = -2.02 \pm 0.08 \quad (28)$$

with a conservatively determined error bar (there is significant curvature present in the second and fourth curves in figure 9). This result is consistent with the estimated value in equation (27). Using this result with the estimate of  $\gamma_{21}$  gives  $2\gamma_{21} - \gamma_{211} = 0.18(10)$ . Within its large error bar, this result is consistent with  $\gamma = 0.15695300(95)$  [26] as shown by equation (13).

The estimates for grafted 2-star exponents are listed in table III.

Data for grafted 3-, 4- and 5-stars were similarly analysed and the results appear in table III. In the case of grafted 3-stars, the estimates are

$$\begin{aligned} \gamma_{30} &= -0.521 \pm 0.002, \\ \gamma_{31} &= -1.59 \pm 0.02, \\ \gamma_{311} &= -2.68 \pm 0.07, \\ \gamma_{3111} &= -3.9 \pm 0.6. \end{aligned} \quad (29)$$

The estimate for  $\gamma_{3111}$  is based on data for  $206 \leq n \leq 1080$ . These results are consistent with equation (11). Using equation (11) and the estimates for  $\gamma_{30}$ ,  $\gamma_{31}$  and  $\gamma_{311}$  gives a better estimate of  $\gamma_{3111}$  instead:

$$\gamma_{3111} = \gamma_{30} - 3\gamma_{31} + 3\gamma_{311} = -3.8 \pm 0.3, \quad (30)$$

and this result is still consistent with the estimate of  $\gamma_{3111}$  in equation (29).

The data for grafted 4s-stars give

$$\begin{aligned} \gamma_{40} &= -1.325 \pm 0.004, \\ \gamma_{41} &= -2.406 \pm 0.008, \\ \gamma_{411} &= -3.48 \pm 0.04, \\ \gamma_{4111} &= -4.6 \pm 0.2. \end{aligned} \quad (31)$$

The estimate for  $\gamma_{4111}$  is based on  $206 \leq n \leq 1650$ . By equation (11),

$$\gamma_{41111} = -\gamma_{40} + 4\gamma_{41} - 6\gamma_{411} + 4\gamma_{4111} = -5.8 \pm 1.1. \quad (32)$$

Finally, for grafted 5-stars

$$\begin{aligned} \gamma_{50} &= -2.251 \pm 0.003, \\ \gamma_{51} &= -3.333 \pm 0.007, \\ \gamma_{511} &= -4.41 \pm 0.04, \\ \gamma_{5111} &= -5.5 \pm 0.2. \end{aligned} \quad (33)$$

Our sampling of 51111- and 511111-stars were too poor to allow estimates of the entropic exponents.

## CONCLUSIONS

The purpose of this paper was to estimate the entropic exponents of half-space grafted  $f$ -stars, and to numerically verify some relations involving these exponents. Our results are shown in tables II and III, Barber's scaling relation is tested in equations (18) and (24), and equations (12) and (13) were tested in equations (19) and (25). The relation in equation (13) was similarly tested for grafted 2-stars and 3-stars in the half cubic lattice (equations (27) and (28), and (29) and (30)). In all respects the general framework using vertex exponents  $\sigma_f$  and surface vertex exponents  $\sigma'_f$  in equation (5) is strongly supported by the numerical results here.

The results in two dimensions are consistent to good accuracy with the exact (conformal invariance) values of the exponents. This not only provides strong evidence supporting the theoretical analysis of the surface entropic exponents for uniform branched networks in two dimensions in references [18, 19, 21, 22], but also shows that the numerical methods used in this paper (and in references [13, 15, 23, 33]) are sound. This enhances confidence in the cubic lattice results shown here, which cannot be verified against a list of exact values. On the contrary, few of the surface exponents of grafted lattice stars in three dimensions have been calculated before (as can be seen in table III), apart from the  $O(\epsilon)$ -expansion estimates which give good, but not excellent, agreement with the numerical estimates obtained in this paper.

## Acknowledgements

EJJvR acknowledges financial support from NSERC (Canada) in the form of Discovery Grant RGPIN-2019-



06303 and is in debt to N Clisby for useful feedback on an earlier version of the manuscript.

- 
- [1] JM Hammersley and KW Morton. Poor man's Monte Carlo. *J Roy Stat Soc Ser B (Meth)*, 16:23–38, 1954.
- [2] SR Broadbent and JM Hammersley. Percolation processes I. crystals and mazes. *Proc Camb Phil Soc*, 53:629–641, 1957.
- [3] CE Soteris. Lattice models of branched polymers with specified topologies. *J Math Chem*, 1:91–102, 1993.
- [4] SG Whittington and CE Soteris. Uniform branched polymers in confined geometries. *Macromol Rep*, 29(S2):195–199, 1992.
- [5] M-N Chee and SG Whittington. The growth constant of uniform star polymers in a slab geometry. *J Phys A: Math Gen*, 20:4915–4921, 1987.
- [6] N Clisby and I Jensen. A new transfer-matrix algorithm for exact enumerations: Self-avoiding polygons on the square lattice. *J Phys A: Math Theor*, 45:115202, 2012.
- [7] N Clisby. Calculation of the connective constant for self-avoiding walks via the pivot algorithm. *J Phys A: Math Theo*, 46:245001, 2013.
- [8] A Miyake and KF Freed. Internal chain conformations of star polymers. *Macromolecules*, 17:678–683, 1984.
- [9] JEG Lipson, SG Whittington, MK Wilkinson, JL Martin, and DS Gaunt. A lattice model of uniform star polymers. *J Phys A: Math Gen*, 18:L649–473, 1985.
- [10] J Batoulis and K Kremer. Thermodynamic properties of star polymers: Good solvents. *Macromolecules*, 22:4277–4285, 1989.
- [11] B Duplantier and AJ Guttmann. Statistical mechanics of confined polymer networks. *J Stat Phys*, 180:1061–1094, 2020.
- [12] K Ohno and K Binder. Monte Carlo simulation of many-arm star polymers in two-dimensional good solvents in the bulk and at a surface. *J Stat Phys*, 64:781–806, 1991.
- [13] P Grassberger. Nonuniform star polymers in two dimensions. *J Phys A: Math Gen*, 27:L721–L725, 1994.
- [14] K Ohno. Scaling theory and computer simulation of star polymers in good solvents. *Cond Mat Phys*, 5:15–36, 2002.
- [15] H-P Hsu, W Nadler, and P Grassberger. Scaling of star polymers with 1-80 arms. *Macromol*, 37:4658–4663, 2004.
- [16] S Campbell and EJ Janse van Rensburg. Numerical estimates of square lattice star vertex exponents. *Phys Rev E*, 103:052137, 2021.
- [17] S Campbell and EJ Janse van Rensburg. Lattice star and acyclic branched polymer vertex exponents in 3d. *Journal of Physics A: Mathematical and Theoretical*, 55(1):015002, 2021.
- [18] JL Cardy. Conformal invariance. In C Domb and JL Lebowitz, editor, *Phase Transitions and Critical Phenomena*, volume 11, pages 55–126. Academic Press, 1983.
- [19] B Nienhuis. Coulomb gas description of 2-D critical behaviour. *J Stat Phys*, 34:731–761, 1984.
- [20] N Clisby and B Dünweg. High-precision estimate of the hydrodynamic radius for self-avoiding walks. *Phys. Rev. E*, 94:052102, 2016.
- [21] B Duplantier. Polymer network of fixed topology: renormalization, exact critical exponent  $\gamma$  in two dimensions, and  $d = 4 - \epsilon$ . *Phys Rev Lett*, 57:941–944, 1986.
- [22] B Duplantier. Statistical mechanics of polymer networks of any topology. *J Stat Phys*, 54:581–680, 1989.
- [23] P Grassberger. Simulations of grafted polymers in a good solvent. *J Phys A: Math Gen*, 38:323–331, 2005.
- [24] R Guida and J Zinn-Justin. Critical exponents of the  $n$ -vector model. *J Phys A: Math Gen*, 31:8103–8122, 1998.
- [25] RD Schramm, GT Barkema, and RH Bisseling. Exact enumeration of self-avoiding walks. *J Stat Mech: Theo Expr*, 2011:P06019, 2011.
- [26] N Clisby. Scale-free Monte Carlo method for calculating the critical exponent  $\gamma$  of self-avoiding walks. *J Phys A: Math Theo*, 50:264003, 2017.
- [27] MN Barber. Scaling relations for critical exponents of surface properties of magnets. *Phys Rev B*, 8:407–409, 1973.
- [28] MN Barber, AJ Guttmann, KM Middlemiss, GM Torrie, and SG Whittington. Some tests of scaling theory for a self-avoiding walk attached to a surface. *J Phys A: Math Gen*, 11(9):1833–1842, 1978.
- [29] B Duplantier and H Saleur. Exact surface and wedge exponents for polymers in two dimensions. *Phys Rev Lett*, 57:3179–3182, 1986.
- [30] H Meirovitch and I Chang, I. Surface critical exponents of self-avoiding walks on a square lattice with an adsorbing linear boundary: A computer simulation study. *Phys Rev E*, 48(3):1960–1969, 1993.
- [31] S Livne and H Meirovitch. Computer simulation of long polymers adsorbed on a surface I. Corrections to scaling in an ideal chain. *J Chem Phys*, 88:4498–4506, 1988.
- [32] H Meirovitch and S Livne. Computer simulation of long polymers adsorbed on a surface II. Critical behavior of a single self-avoiding walk. *J Chem Phys*, 88:4507–4515, 1988.
- [33] R Hegger and P Grassberger. Chain polymers near an adsorbing surface. *J Phys A: Math Gen*, 27:4069–4081, 1994.
- [34] N Clisby, AR Conwar, and AJ Guttmann. Three-dimensional terminally attached self-avoiding walks and bridges. *J Phys A: Math Theo*, 49:015004, 2016.
- [35] N Clisby. Accurate estimate of the critical exponent  $\nu$  for self-avoiding walks via a fast implementation of the pivot algorithm. *Phys Rev Lett*, 104:055702, 2010.
- [36] K Binder, C Domb, and MS Green. Critical behaviour at surfaces. In C Domb and JL Lebowitz, editor, *Phase Transitions and Critical Phenomena*, volume 8, pages 1–144. Academic Press, 1983.
- [37] K Binder and DP Landau. Critical phenomena at surfaces. *Physica A*, 163:17–30, 1990.
- [38] P Grassberger. Pruned-enriched Rosenbluth method: Simulations of  $\theta$  polymers of chain length up to 1,000,000. *Phys Rev E*, 56:3682–3693, 1997.
- [39] H-P Hsu and P Grassberger. A review of Monte Carlo simulations of polymers with perm. *J Stat Phys*, 144:597–637, 2011.
- [40] T Prellberg and J Krawczyk. Flat histogram version of the pruned and enriched Rosenbluth method. *Phys Rev Lett*, 92:120602, 2004.
- [41] S Campbell and EJ Janse van Rensburg. Parallel PERM. *J Phys A: Math Theo*, 2020.
- [42] M Matsumoto and T Nishimura. Mersenne twister: A 623-dimensionally equidistributed uniform pseudo-random number generator. *ACM Trans Mod Comp Sim (TOMACS)*, 8(1):3–30, 1998.

- [43] F Panneton, P L'Ecuyer, and M Matsumoto. Improved long-period generators based on linear recurrences modulo 2. *ACM Trans Math Software*, 32:1–16, 2006.
- [44] B Nienhuis. Exact critical point and critical exponents of  $O(n)$  models in two dimensions. *Phys. Rev. Lett.*, 49:1062–1065, 1982.
- [45] S Caracciolo, AJ Guttmann, I Jensen, A Pelissetto, AN Rogers, and AD Sokal. Correction-to-scaling exponents for two-dimensional self-avoiding walks. *J Stat Phys*, 120:1037–1100, 2005.
- [46] T Williams, C Kelley, et al. Gnuplot 4.6: An interactive plotting program. <http://gnuplot.sourceforge.net/>, 2013.